Comparison of yields of neutron-rich nuclei in proton- and photon-induced ^{238}U fission

F. A. Khan,[1,2,*] Debasis Bhowmick,[2,†] D. N. Basu,[2,‡] M. Farooq,[1,§] and Alok Chakrabarti[2,‖]
[1]*Dept. of Physics, University of Kashmir, Hazratbal, Srinagar 190 006, India*
[2]*Variable Energy Cyclotron Centre, 1/AF Bidhan Nagar, Kolkata 700 064, India*
(Received 5 July 2016; revised manuscript received 27 September 2016; published 7 November 2016)

A comparative study of fission of actinides, especially ^{238}U, by proton and bremsstrahlung photon is performed. The relative mass distribution of ^{238}U fission fragments has been explored theoretically for both proton- and photon-induced fission. The integrated yield along with charge distribution of the products are calculated to find the neutron richness in comparison with the nuclei produced by the *r* process in nucleosynthesis. Some *r*-process nuclei in the intermediate-mass range for symmetric fission mode are found to be produced almost two orders of magnitude more for proton-induced fission than for photofission, although the rest of the neutron-rich nuclei in the asymmetric mode are produced in comparable proportion for both processes.

DOI: 10.1103/PhysRevC.94.054605

I. INTRODUCTION

Fission of actinide targets, especially uranium or thorium, is a highly promising route for producing neutron-rich (*n*-rich) radioactive ion beams (RIBs) for nuclear spectrometry. Fission by neutron [1], proton [2], and photon [3,4] has been studied for several decades and is still relevant. Among these three, photofission [5] has been found more promisingbecause it offers better thermal management and is a cold process that creates higher yields for *n*-rich nuclei as compared with light-ion-induced fission, except in the mass range of $110 < A < 125$. Therefore, there is a renewed interest presently to go for photofission [6] by using e-LINAC as a primary accelerator to produce energetic photons in the giant dipole resonance (GDR) region [7,8]. The Advanced Rare Isotope Laboratory (ARIEL) [9,10] at TRIUMF, JINR, Dubna [11] and at ALTO, IPN, Orsay [12] are the laboratories where initiatives have already been taken. As an extension of the present RIB development, a facility called the Advanced National Facility for Unstable and Rare Isotope Beams (ANURIB) [13] will be coming up at this center with e-LINAC as the primary accelerator for photofission. However, it is true that low-energy proton-induced fission also provides relatively less expensive means to produce *n*-rich nuclei substantially in a specific mass region. For this, one can have low-energy proton beams (either from a cyclotron or a proton LINAC) instead of an e-LINAC, so that *n*-rich RIBs, produced in a second target station be put subsequently in the same postaccelerator module.

It is well known that the properties of fission-mass distribution is governed by asymmetric and symmetric mass split of the fissioning nuclei, depending on the excitation energy. In the energy range 12–30 MeV, ^{238}U fission is known to take place in both asymmetric and symmetric fission modes with comparable probabilities [14]. However, the probability of asymmetric fission relative to that of symmetric fission decreases with proton energies. For very high energy (100 MeV), the mass-yield curve does not have any trough, although the total fission cross section remains constant after 30 MeV [15]. In neutron- and photon-induced fission, at low energies, the pattern of mass distribution of the products are found to be nearly identical with that of proton-induced fission. However, in case of photofission, the *n*-rich nuclei produced in symmetric fission mode have a much lower cross section compared with the two asymmetric modes, and increasing the excitation energy does not help because the total cross section decreases rapidly due to the absence of the giant dipole resonance, unlike proton-induced fission where the increase of the symmetric fission mode is compensated by reduction in the asymmetric mode, so that the total fission cross section remains unchanged after 30 MeV. Therefore, in the present work, we simultaneously analyze the behavior of the symmetric and asymmetric modes of proton-induced fission for different excitation energies of ^{238}U, and a comparison with that of photofission is made. Depending on the availability of data, the analysis can also be be extended to other actinides (Th, Pu, Am, Np, etc.). TALYS [16] and PACE4 [17] results are also incorporated into the comparison for the calculation of total cross section of proton-induced fission along with experimental data because both codes take into account the competition of other reaction channels in addition to fission. Finally, the role of proton-induced fission of actinides, especially ^{238}U, towards the production of *n*-rich nuclei in the mass range $110 < A < 125$ is explored.

II. THEORETICAL FORMALISM OF FISSION CROSS SECTION

The empirical formula employed in our calculation is taken from Ref. [18] as

$$\sigma_f(E_p) = P_1\{1 - \exp[-P_2(E_p - P_3)]\}, \qquad (1)$$

where σ_f, is the total fission cross section (mb), and E_p is the incident proton energy (MeV). P_i $(i = 1,2,3)$ are the arbitrary fitting parameters with the physical meaning that P_1 is the saturation cross section, P_2 is the increasing rate of cross section with energy, and P_3 is the apparent threshold energy.

*29firdous11@gmail.com
†dbhowmick@vecc.gov.in
‡dnb@vecc.gov.in
§farooq@gmail.com
‖alok@vecc.gov.in

The P_i have been parametrized with the fissility parameter Z^2/A as

$$P_i(Z^2/A) = \exp[Q_{i,1} + Q_{i,2}(Z^2/A) + Q_{i,3}(Z^2/A)^2], \quad (2)$$

where Q_i are the coefficients of the powers of (Z^2/A), which are also determined by fitting the experimental fission cross-section data for a wide range of fissioning nucleus from ^{181}Ta to ^{181}Bi as shown by Fukahori and Pearlstein [19]. However, later on Fukahori and Chiba [20] modified the expression where the fission probability was calculated as the ratio of experimental fission cross section and the total reaction cross section, as calculated by Letaw [21]. With the availability of precise data of fission cross sections from time to time, the systematics improved quite a lot. Systematics used by Prokofiev [18] is found to be very effective in the energy range 12–63 MeV for calculating total fission cross section σ_f as described in Eq. (2) by fitting experimental data [22,23], while P_1 is parametrized differently as

$$P_1(Z^2/A) = R_{11}\{1 - \exp[-R_{13}(Z^2/A - R_{12})]\}. \quad (3)$$

It is important to mention here that we have not considered here the high-energy correction term because it is effective for proton energy in the range of hundreds of MeV or more. The values of $P_2 = 0.111$ and $P_3 = 12.1$ are considered to be constant since, from Ref. [19], it is found to be invariant for Z^2/A in the range 35.9 to 36.1 for ^{132}Th–^{239}Pu. The values of $R_1 j$ $(j = 1–3)$ are fit by a least-squares fit and found to be $R_{11} = 2730 \pm 82.962$, $R_{12} = 34.99 \pm 0.034$, and $R_{13} = 2.07 \pm 0.120$.

III. SYSTEMATICS OF MASS AND CHARGE DISTRIBUTION

Although we have tried to accumulate the data to date as much as possible [24,25], the availability of data for both fission cross section and mass distribution are not too many in the energy range of 13–60 MeV. In general, the mass distribution is interpreted as a sum of the contribution from the symmetric and asymmetric fission modes for the multimode fission model. Each fission mode corresponds to the passage through the fission barrier of specific shape. For each fission mode, the yield is described in the form of a Gaussian function. Three Gaussian functions are found to be good enough for describing two fission modes. The symmetric fission mode (SM) is peaked around $A = 118$, while for asymmetric fission modes (ASYM), the maxima are at $A = 137$ and $A = 99$. The total yield of fragments whose mass number is A is given by the expression

$$\begin{aligned} Y(A) &= Y_{\mathrm{SM}}(A) + Y^1_{\mathrm{ASYM}}(A) + Y^2_{\mathrm{ASYM}}(A) \\ &= C_{\mathrm{SM}} \exp\left[-\frac{(A - A_{\mathrm{SM}})^2}{2\sigma^2_{\mathrm{SM}}}\right] \\ &\quad + C_{\mathrm{ASYM}} \exp\left[-\frac{(A - A_{\mathrm{SM}} - D_{\mathrm{ASYM}})^2}{2\sigma^2_{\mathrm{ASYM}}}\right] \\ &\quad + C_{\mathrm{ASYM}} \exp\left[-\frac{(A - A_{\mathrm{SM}} + D_{\mathrm{ASYM}})^2}{2\sigma^2_{\mathrm{ASYM}}}\right], \end{aligned} \quad (4)$$

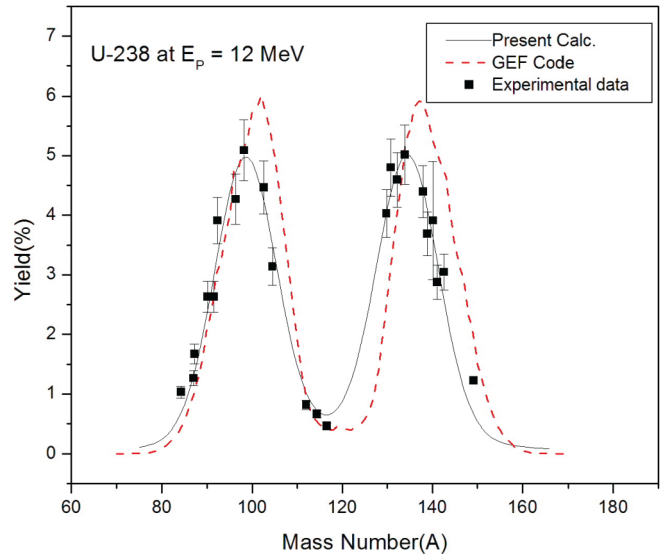

FIG. 1. Comparison of the measured mass-yield distribution (solid squares) [24] for ^{238}U fission induced by 12 MeV protons with the prediction (solid line) of the three-Gaussian formula for $Y(A)$ and GEF predictions [26].

where the Gaussian function parameters C_{SM}, C_{ASYM} and σ_{SM}, σ_{ASYM} are the amplitudes and widths, respectively, of the symmetric (SM) and asymmetric (ASYM) fission modes, and A_{SM} is the most probable mass value for the symmetric fission mode while $A_{\mathrm{SM}} - D_{\mathrm{ASYM}}$ and $A_{\mathrm{SM}} + D_{\mathrm{ASYM}}$ are the most probable masses of a light and the complementary heavy fragments, respectively, in the asymmetric fission mode.

In Figs. 1 and 2, approximation by the preceding three-Gaussian functions for the mass distribution $Y(A)$ of fragments per 100 fission events originating from ^{238}U fission induced by 12 and 35 MeV protons are plotted and compared with

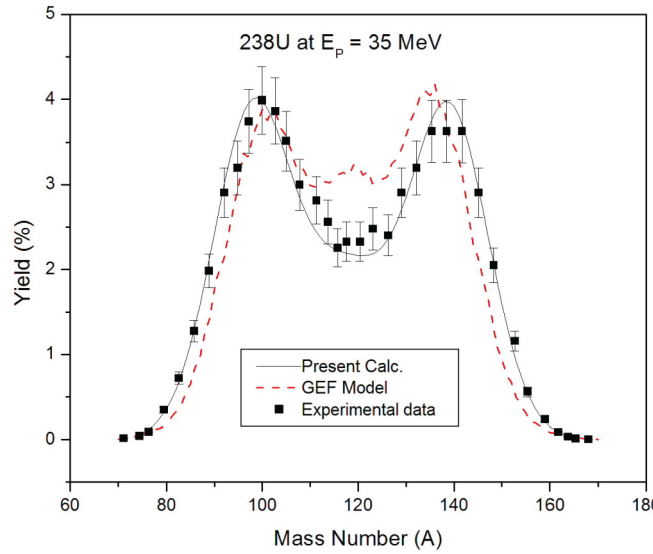

FIG. 2. Same as Fig. 1 (solid squares) [25] but for a different proton energy of 35 MeV.

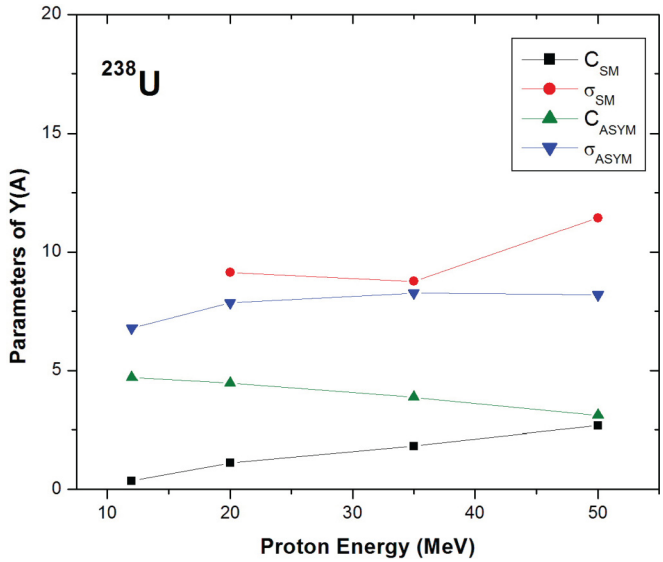

FIG. 3. Variation of symmetric and asymmetric Gaussian parameters with excitation energies.

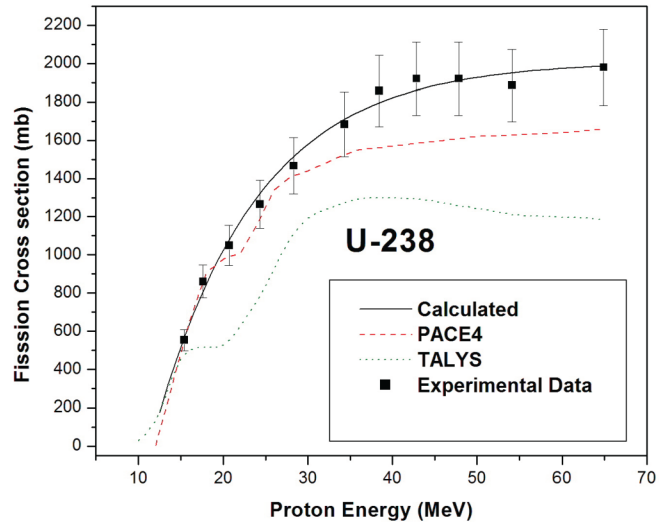

FIG. 4. Comparison of total fission cross section (solid squares) [22,23] of ^{238}U by protons with energies in the range 13–63 MeV with the prediction (solid line) from our calculation, TALYS and PACE4.

experimental data in Refs. [24,25], respectively, as well as with the theoretical predictions of GEF calculations [26]. It is important to mention here that, with increasing energy, the amplitude of both the asymmetric peak decreases, although not so appreciably in the energy domain considered here. However, as far as symmetric fission is concerned, the increase is substantial. Therefore, the probability of symmetric fission relative to that of symmetric fission decreases appreciably with increasing proton energy. The values of $A_{\rm SM}$, $D_{\rm ASYM}$ are 118 and 19, respectively, whereas the variation of four other parameters with proton energy ranging from 12 to 50 MeV are plotted in Fig. 3. The lines represent least-square fits assuming quadratic energy dependence of the parameters. It is important to note that the value of $\sigma_{\rm SM}$ at 12 MeV is not shown in Fig. 3 because of large error due to insufficient experimental data points. Furthermore, the percentage yield of isotopes having mass number in the range 115–120 are very small and due to which the fitted mean value of $\sigma_{\rm SM}$ is found to be very high (e.g., $\sigma_{\rm SM} = 27.7 \pm 14.2$ for Fig. 1). In fact, at such a low energy, fission of ^{238}U is perfectly asymmetric and one can fit with two Gaussian functions leaving aside the symmetric term in the expression of mass-yield distribution $Y(A)$ in Eq. (4).

The isobaric charge distribution of photofission products can be well simulated by a single Gaussian function as

$$Y(A,Z) = \frac{Y(A)}{\sqrt{\pi C_p}} \exp\left[-\frac{(Z - Z_s)^2}{C_p}\right], \qquad (5)$$

where Z_s represents the most stable isotope of fission fragment with mass number A. To deduce an expression for Z_s, theoretically, for the most-stable nucleus by keeping mass number A constant while differentiating the liquid drop model mass formula and setting the term $\partial M_{\rm nucleus}(A,Z)/\partial Z\,|_A$ equal to zero as described in Ref. [27]. The value of the parameter C_p which decides the dispersion for the most probable isotope is extracted by fitting experimental data [22] is found to be 0.95. In the present work the form of the charge distribution is assumed to be independent of the mass number of the actinides and proton energy for the range considered here. The atomic numbers Z_s used in Eq. (5) for the most stable nuclei are calculated by using the values $a_c = 0.71$ MeV and $a_{\rm asym} = 23.21$ MeV [27].

IV. CALCULATION AND RESULTS

The production cross sections of individual fission fragments induced by protons are obtained by multiplying fission cross section $\sigma_f(E_p)$, as calculated by the empirical formula in Eq. (1), by charge distribution which means $\sigma_f(A,Z) = \sigma_f(E_p)Y(A,Z)/100$.

It is important to mention here that total fission cross section $\sigma_f(E_p)$ increases with increasing proton energy, but it saturates almost at 30 MeV. However, for photofission, the cross section maximizes in the GDR range for mean photon energy of 13.7 MeV. In Fig. 4, $\sigma_f(E_p)$ vs proton energy has been plotted by using PACE4 [17] and TALYS [16] along with our empirical formalism to compare with experimental data [22,23]. In an attempt to make a comparison of proton-induced fission with photofission, the choice of energy of the incident particle (proton or photon) is made such that the fission cross section is maximized.

In Figs. 5 and 6, the ratio of cross sections of proton- and photon-induced fission at energies 35 and 13.7 MeV, respectively, as $(\sigma_p^{35}/\sigma_\gamma^{13.7})$ for two different A/Z at 2.50 and 2.66 are plotted for a range of fragment mass number from 80 to 150. It is evident from Fig. 5 that, in general, the proton-induced fission cross section is an order magnitude higher than photofission in the asymmetric mode, while in the symmetric fission mode the order of enhancement is more than 70–90 times. Moreover, because A/Z of fissioning nuclei increases the peak value of the ratio shifts towards lower mass number in the symmetric fission mode. For $A/Z = 2.50$ the

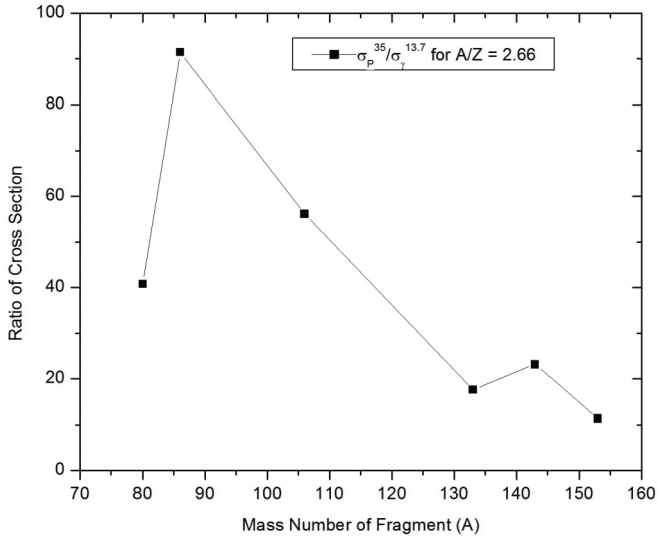

FIG. 5. Variation of ratio of cross sections (35 MeV p/13.7 MeV photon) with fragment mass number for $A/Z = 2.66$.

ratio of the cross-section peaks around A (product) $= 120$, while for $A/Z = 2.66$ it is around 96 (Figs. 5 and 6).

In Fig. 7, a comparison between proton-induced fission and photofission of ^{238}U has been carried out in a different way where the ratio of proton- and γ-induced fission cross sections are shown by contour plots in the neutron number (N) and atomic number (Z) plane. The cross sections for most neutron-rich isobars are calculated with proton and mean photon energy of 35 and 13.7 MeV, respectively. For the same mass number, the ratios of cross sections are found be constant and hence, in the N-Z plane, these appear as straight lines. It is evident from Fig. 7 that the enhancement of the ratio of cross section ($\sigma_p^{35}/\sigma_\gamma^{13.7}$) is substantially of the order of $\sim$80 in the mass range $A = 110$–125. However, the two fringes at

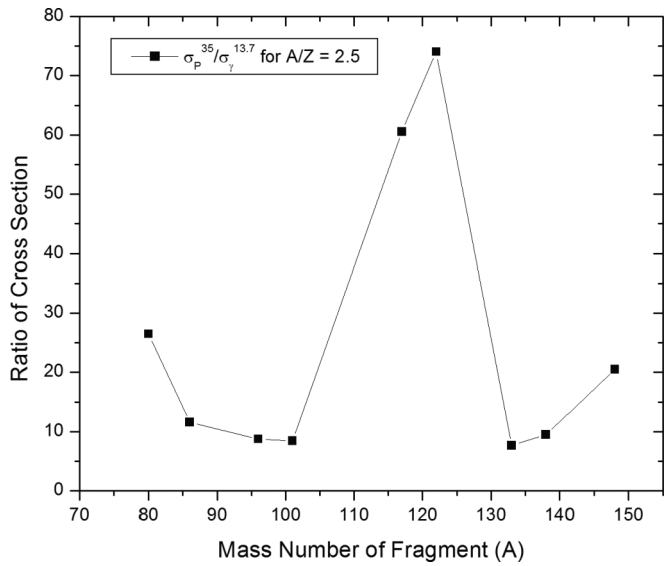

FIG. 6. Same as Fig. 5 but for $A/Z = 2.5$.

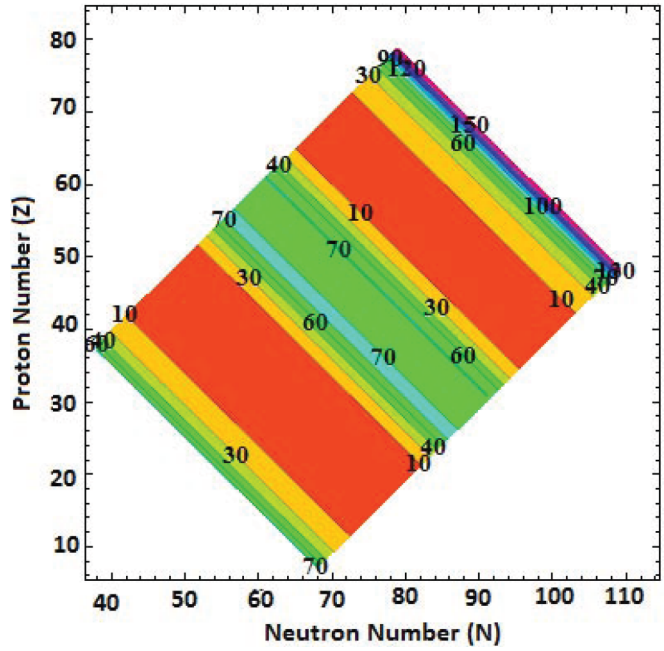

FIG. 7. Two-dimensional contour plots for the ratio of proton- and γ-induced ^{238}U fission cross sections vs atomic number Z and neutron number N. These ratios are represented by different color shades corresponding to the different values mentioned in the figure.

$A = 60$ and at $A = 160$, it shoots up to $\sim$160, while for the remaining masses it is of the order of $\sim$10.

The experimentally observed β-stable nuclei along with the r-process nuclei are also shown in Fig. 8 to highlight how much one can march away from β stability towards the r-process path by using ^{238}U proton- and photon-induced fission. Although there is no significant difference between proton- and photon-induced fission so far as production of neutron-rich nuclei is concerned, still proton-induced fission is a little ahead towards the n-drip line than the other one.

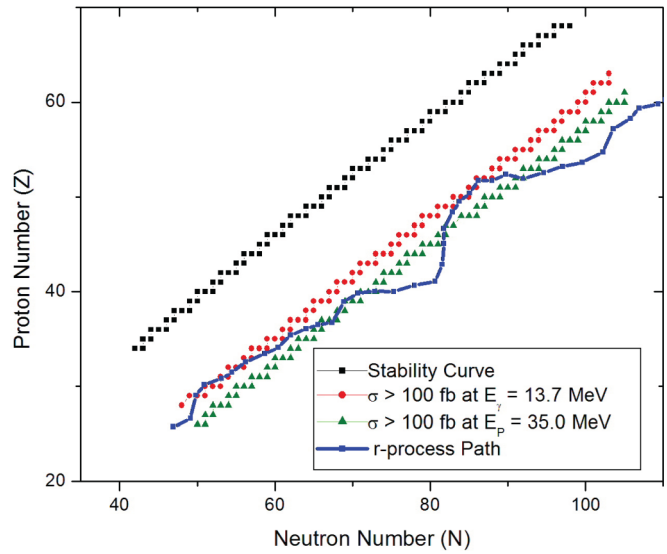

FIG. 8. Plots of atomic number Z vs neutron number N for exotic nuclei produced by photon- and proton-induced fission of ^{238}U.

TABLE I. Theoretical cross sections for production of nuclei with same A/Z.

Nuclei	A/Z	Z_s	A_s	Z_s-Z	$A^F-A_s^F$	$\sigma_\gamma^{13.7}$ (mb)	σ_P^{35} (mb)	$\sigma_P^{35}/\sigma_\gamma^{13.7}$
^{80}Zn	2.66	36	64	6	16	2.6×10^{-3}	1.1×10^{-1}	40.00
^{96}Kr	2.66	42	84	6	12	2.1×10^{-3}	1.9×10^{-1}	91.43
^{106}Zr	2.66	46	91	6	15	3.9×10^{-3}	2.2×10^{-1}	56.15
^{133}Sn	2.66	56	119	6	14	2.2×10^{-3}	3.9×10^{-2}	17.59
^{143}Xe	2.66	60	131	6	12	6.6×10^{-3}	1.5×10^{-1}	23.18
^{154}Ce	2.66	64	140	6	14	2.2×10^{-3}	2.5×10^{-2}	11.32

In an effort to investigate the production cross section of neutron-rich nuclei by proton- and photon-induced fission, some isotopes with maximum cross section (appearing at the two asymmetric peaks of the mass distributions), some with small lower cross section (appearing at the symmetric mass distribution) are arranged in Table I with proton and average photon energies 35 and 13.7 MeV, respectively. It is evident from Table I that relative enhancement in proton-induced fission over photons is substantially high for products in the symmetric mass distribution domain (e.g., for ^{122}Cd). Moreover, in Table II, the production cross sections of some r-process nuclei are highlighted where cross sections are tabulated both for proton- and photon-induced fission. For some waiting-point nuclei, e.g., ^{80}Zn and ^{134}Sn, the production cross sections are enhanced by 40 and 20 times, respectively, by proton- than to photon-induced fission. Comparing Tables I and II, one may notice that, for A/Z almost equal to 2.55 ± 0.01, when $Z_s - Z = 4$, the cross sections are a few tens of milibarns, while for A/Z almost equal to 2.66, when $Z_s - Z = 6$ the cross sections reduce to one tenth of a microbarn for proton-induced fission of ^{238}U. The reduction of cross section is consistent because cross sections fall rapidly with increasing mass number because of the neutron richness that is obvious from Eq. (5).

V. SUMMARY AND CONCLUSION

In summary, we find that the two-mode fission mechanism with three-Gaussian function along with four arbitrary parameters behave quite satisfactorily on the observed mass yield curve for proton-induced fission of ^{238}U up to 60 MeV. The empirical formalism nicely reproduces the total fission cross section for fission of various actinide elements over a wide range of incident proton energy and, in the high-energy domain especially, it fits better than TALYS and PACE4 codes, where competition from other reaction channels is considered in addition to fission.

As far as the production of neutron-rich nuclei is concerned, comparisons have been carried out between proton- and photon-induced fission of ^{238}U. The present calculation indicates clearly that many of the r-process nuclei in intermediate mass range can be obtained in the laboratory with measurable cross section both by proton- and photon-induced fission and, to be precise, it is better by proton-induced fission than by photon-induced fission, although not much significant. Sometime, the betterment is almost two orders of magnitude in the mass range 110–125 in the symmetric fission mode for incident proton energy more than 35 MeV. However, production of r-process nuclei through photon-induced fission (bremsstrahlung photons from energetic electrons by e-LINAC) is preferred because of better thermal management in the target design by having two targets (converter target and fission target) instead of one. But keeping a simultaneous option for proton-induced fission may be a judicious choice if one really requires producing nuclei such as ^{117}Pd , ^{122}Cd (8- to 9-neutron excess) or more neutron-rich nuclei such as ^{80}Zn , ^{96}Kr, and ^{106}Zr (15- to 16-neutron excess).

Finally, for producing neutron-rich nuclei, in the higher mass range, more than $A = 160$, one would need to go for the proton-induced reaction rather than the nuclear process other than a photonuclear reaction to produce them and, for that, a high-energy proton beam is required.

TABLE II. Theoretical cross sections for production of some r-process nuclei.

Nuclei	A/Z	Z_s	A_s	Z_s-Z	$A^F-A_s^F$	$\sigma_\gamma^{13.7}$ (mb)	σ_P^{35}(mb)	$\sigma_P^{35}/\sigma_\gamma^{13.7}$
^{80}Ge	2.50	36	74	4	6	1.2×10^{-1}	3.07	26.53
^{86}Se	2.52	38	80	4	6	1.1×10^{0}	12.42	11.62
^{96}Sr	2.53	42	88	4	8	4.4×10^{0}	38.38	8.77
^{101}Zr	2.53	44	90	4	11	4.8×10^{0}	40.74	8.46
^{117}Pd	2.54	50	106	4	9	3.3×10^{-1}	19.86	60.56
^{122}Cd	2.54	114	84	4	8	2.9×10^{-1}	21.52	74.04
^{133}Te	2.56	56	128	4	5	3.7×10^{0}	28.55	7.68
^{138}Xe	2.55	58	132	4	6	3.9×10^{0}	37.89	9.53
^{148}Ce	2.55	62	138	4	10	1.1×10^{0}	22.77	20.50

[1] H. Naik, F. Carre, G. N. Kim, F. Laine, A. Sari, S. Normand, and A. Goswami, Eur. Phys. J. A **49**, 94 (2013).
[2] A. Deppman, E. Andrade-II, V. Guimarães *et al.*, Phys. Rev. C **88**, 064609 (2013).
[3] B. S. Ishkhanov and A. A. Kuznetsov, Phys. At. Nucl. **77**, 824 (2014).
[4] S. S. Belyshev, B. S. Ishkhanov, A. A. Kuznetsov, and K. A. Stopani, Phys. Rev. C **91**, 034603 (2015).
[5] S. Essabaa *et al.*, Nucl. Instrum. Methods Phys. Res., Sect. B **204**, 780 (2003).
[6] W. T. Diamond, Nucl. Instrum. Methods Phys. Res., Sect. A **432**, 471 (1999).
[7] D. Bhowmick, D. Atta, D. N. Basu, and A. Chakrabarti, Phys. Rev. C **91**, 044611 (2015).
[8] D. Bhowmick, F. A. Khan, D. Atta, D. N. Basu, and A. Chakrabarti, Can. J. Phys. **94**, 243 (2016).
[9] F. Ames *et al.*, Conf. Proc. C **1205201**, 64 (2012).
[10] J. Richards *et al.*, Conf. Proc. ICALEPCS2011, Grenoble, France (2011), p. 465.
[11] Yu. Ts. Oganessian *et al.*, Nucl. Phys. A **701**, 87 (2002).
[12] M. Cheikh Mhamed *et al.*, Nucl. Instrum. Methods Phys. Res., Sect. B **266**, 4092 (2008).
[13] A. Chakrabarti *et al.*, Nucl. Instrum. Methods Phys. Res., Sect. B **317**, 253 (2013).
[14] W. H. Jones *et al.*, Phys. Rev. **99**, 184 (1955).
[15] P. C. Stevenson *et al.*, Phys. Rev. **111**, 886 (1958).
[16] A. J. Koning, S. Hilaire, and M. C. Duijvestijn, in *Proceedings of the International Conference on Nuclear Data for Science and Technology, 22–27 April 2007, Nice, France* (2008), pp. 211–214; A. J. Koning, S. Hilaire, and S. Goriely, TALYS-1.4, A Nuclear Reaction Program, December 28, 2011.
[17] O. B. Tarasov and D. Bazin, Nucl. Instrum. Methods Phys. Res., Sect. B **204**, 174 (2003).
[18] A. V. Prokofiev *et al.*, Nucl. Instrum. Methods Phys. Res., Sect. A **463**, 557 (2001).
[19] T. Fukahori and S. Pearlstein, *Proc. of Advisory Group Meeting Organized by IAEA, Vienna, October 9–12, 1990*, IAEA Report INDC(ND5)-245 (1991), p. 93.
[20] T. Fukahori and S. Chiba, *Proc. of the First Internet Symposium on Nuclear Data, April 8 - June 15, 1996, JAERI, Tokai, Ibaraki, Japan*: Paper No. 09; JAERI-Conf 97-004, INDC(JPN)-178/U, p. 95.
[21] J. R. Letaw, R. Silberberg, and C. H. Taso, Astrophys. J., Suppl. Ser. **51**, 271 (1983).
[22] S. Baba *et al.*, Nucl. Phys. A **175**, 177 (1971).
[23] S. Isaev *et al.*, Nucl. Phys. A **809**, 1 (2008).
[24] T. Ohtsuki, Y. Hamajima, K. Sueki, H. Nakahara, Y. Nagame, N. Shinohara, and H. Ikezoe, Phys. Rev. C **40**, 2144 (1989).
[25] V. A. Rubchenya *et al.*, Nucl. Instrum. Methods Phys. Res., Sect. A **463**, 653 (2001).
[26] K.-H. Schmidt, B. Jurado, and C. Amouroux, JEFF-Report 24 of the Nuclear-Energy Agency of the OECD (2016).
[27] P. Roy Chowdhury and D. N. Basu, Acta Phys. Pol., B **37**, 1833 (2006).